Adv. Nat. Sci.: Nanosci. Nanotechnol. **5** (2014) 035007 (12pp) doi:10.1088/2043-6262/5/3/035007

Tunable morphological properties of silver enriched platinum allied nanoparticles and their catalysed reduction of p-nitrophenol

Joseph Adeyemi Adekoya[1], **Enock Olugbenga Dare**[2] **and Michael Adediran Mesubi**[3]

[1] Department of Chemistry, Covenant University, P. M. B. 1023, Ota, Ogun State, Nigeria
[2] Department of Chemistry, Federal University of Agriculture, P. M. B. 2240, Alabata Road Abeokuta, Nigeria
[3] Department of Chemistry, Kwara State University, Malete, P. M. B. 1530, Ilorin, Nigeria

E-mail: joseph.adekoya@covenantuniversity.edu.ng

Received 25 April 2014
Accepted for publication 25 June 2014
Published 9 July 2014

Abstract

A robust polymer based and polyol mediated procedure to synthesize nanobimetallic particles has been modified to produce core–shell and alloy Ag/Pt nanoparticles with tunable properties. Novel three-dimensional (3D) quasi nanocubes entangled in nanowebs were produced by rapid solution phase transformation with hot addition of absolute ethanol. The optical characterization showed extinction of plasmon resonance band occurring with incremental feeding ratio of Pt source in all cases. Transmission electron microscope (TEM) and high resolution transmission electron microscope (HRTEM) images revealed that the shape, size and size distribution of as-prepared silver platinum nanoparticles depended on the stabilizer or capping agent, mole ratio of metal ion sources, temperature and time of reaction. Meanwhile, catalytic activity was highest in the reduction of p-nitrophenol in the presence of polyvinylpyrrolidone/diethylene glycol stabilized Ag/Pt nanoparticles.

Keywords: tunable morphological properties, bimetallic nanoparticles, p-nitrophenol
Classification numbers: 2.00, 2.03, 2.04, 4.00

1. Introduction

In the past decades, interest in nanostructures has increased due to their fascinating electronic, chemical, bio-sensing, optical and catalytic properties; as a result, different methods have been developed and deployed to synthesize various nanostructures [1, 2]. Silver nanoparticle in particular has generated a lot of attraction in the sense that it has been investigated based on its significance as a noble metal. The phenomenon of enhanced surface resonance effect has made it a vital material in fibre optics and wave guide or antenna devices. Moreover, silver bimetallic nanoparticles are increasingly attracting further investigation since they lead to unusual size-dependent electrical, chemical and optical properties [3]. Since the optical, electronic and catalytic properties are strongly dependent on the structure and composition of nanomaterials, the synthesis of bimetallic nanostructures with accurately controlled structures and compositions is vital to obtaining such materials with novel and improved properties. It has been reported that the surface plasmon resonance peaks of bimetallic Ag/Pt nanostructures can be readily tuned by controlling the Pt/Ag ratio in the replacement reaction [4].

Although it is widely agreed that nucleation and the ensuing rapid diffusional growth play essential roles in dictating particle morphology, the investigation of these early stages is fraught with major difficulties. Consequently, the mechanisms responsible for the formation of anisometric particles are still not well understood and we are rarely able to predict in previously unexplored systems, which experimental conditions would yield a particular shape.

In a survey of recent work on Ag/Pt bimetallic nanoparticles prepared at various molar ratios by simultaneous reduction of H_2PtCl_6 and $AgNO_3$ with hydrazine in the

microemulsions of water/dioctyl sulfosuccinate sodium salt (AOT)/isooctane at 25 °C [5, 6], the transmission electron microscopy (TEM) images showed that the Ag/Pt bimetallic nanoparticles essentially were monodispersed. Likewise, in the work of Wen-Yin *et al* [7], flexible, transparent and conducting composite thin films were prepared from multi-walled carbon nanotube (MWCNT) supported silver–platinum alloy nanoparticles (Ag/Pt–MWCNT) on a flexible polyethylene terephthalate (PET) substrate, through the combination of a two-step polyol process for synthesizing composites of carbon nanotubes (CNTs) and metallic nanoparticles (NPs) with an ultrasonic atomization-spin coating method for thin films fabrication. Ag/Pt nanoparticles with an average size of approximately 26 nm were uniformly attached to the side walls of MWCNTs forming an effective and strongly mechanical conductive network.

Elsewhere, bimetallic nanoparticles composed of Ag/Pt have been prepared by the successive reduction of $AgNO_3$ and H_2PtCl_6 solutions with hydrazine. It was shown that the surface plasmon resonance peaks corresponding to these composite particles red shifted to longer wavelengths with increasing Pt content, and could possibly get close to the near-infrared region [8]. The water-soluble Ag/Pt core-shell nanoparticles were similarly prepared by deposition Pt over Ag colloidal seeds with the seed-growth method using K_2PtCl_4 with trisodium citrate as reducing agent. The Ag/Pt ratio was varied from 9:1 to 1:3 for synthesizing Pt shell layer of different thickness [9]. Platinum acetylacetonate $Pt(acac)_2$ and silver stearate AgSt were equally used as precursors and diphenyl ether (DPE) as solvent in the preparation of Ag/Pt bimetallic nanoparticles. The TEM results indicated that the formation of twin planes in these Ag/Pt nanoparticles could be the outcome of incorporation of Ag atoms into the Pt lattice [10].

In recent times, the ability of alcohols such as ethanol to act as reducing agents for strongly oxidizing cations has been investigated [11, 12]. Particle agglomeration in such reactions can, however, be problematic, even in the presence of stabilizing agents. The reaction carried out in glycerol, ethane-1, 2-diol or 1, 2-propanediol was found to yield more monodispersed products. This is due to the fact that polyols can effectively act as bidentate chelating agent for the solvated metal cation and at the same time also act as reducing and/or stabilizing agents for the precipitation of nanoparticles.

Herein, we present a polymer-based seed-mediated method for synthesizing well dispersed silver enriched platinum nanoparticles with tunable morphological properties exhibiting the formation of new materials at nanoscale regime in different polyol/polymer matrices and the catalytic reduction of 4-nitrophenol in the presence of sodium borohydride.

2. Experimental

The seed mediated or successive addition method was modified from literature and used to prepare monodispersed bimetallic Ag/Pt nanoparticles in different polyols at optimum concentration of metal precursors and controlled temperature

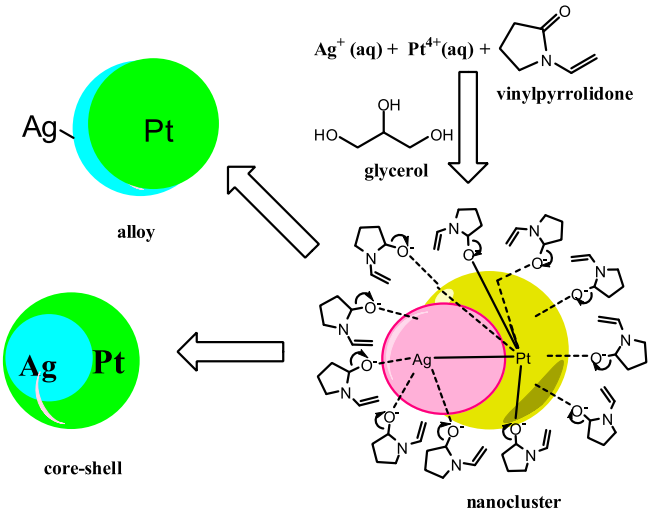

Scheme 1. Mechanism of reaction for the formation of core–shell or alloy Ag/Pt bimetallic nanoparticles.

[13, 14]. The reaction pathway for the formation of bimetallic nanoparticles via anisotropic nucleation and particle growth is shown in scheme 1.

$$PtCl_{4(aq)} + 4Ag_{(s)} \rightarrow Pt_{(s)} + 4Ag^{+}_{(aq)} + 6Cl^{-}_{(aq)}, \quad (1)$$

$$Ag_{(t)} + Pt_{(s)} \rightarrow Ag_{(t)}Pt_{(s)}, \quad (2)$$

where (*aq*) indicates aqueous solution, (*s*)—solid and (*t*)—template.

When $AgNO_3$ solution is reduced by polyol, the formed Ag particles are used as templates for the controlled reduction and deposition of Pt by the template facilitated reaction [15] and/or borohydride reduction. There is excess polyol after the reduction of $AgNO_3$, so the chemically oxidized Ag^+ from replacement reaction (1) will be reduced back to Ag. At the same time, PVP is present as the stabilizer. The long polymeric chain structure of PVP will completely surround one or more nanoparticles and can trap the Ag^+ that is liberated during the displacement reaction, allowing it to combine with $PtCl_4$ and co-reduce near the surface of the template particles [16].

2.1. Materials

All inorganic salts, solvents and chemical reagents used were analytical grade, and were purchased from Sigma-Aldrich Corporation, UK. They are as follows: silver nitrate, platinium (IV) chloride, sodium borohydride, glycerol (GLY), ethylene glycol (EG) and diethylene glycol (DEG), pentaerythritol (PET), poly(vinyl pyrrolidone) (PVP), methanol and ethanol.

2.2. Synthesis of Ag/Pt bimetallic nanoparticles in different polyols

The modified approach to prepare well dispersed tunable property bimetallic Ag/Pt nanoparticles by the seed growth or successive addition method [17, 18] is as follows: 15 mL glycerol (99.5%w w^{-1}) was measured into a round bottom

flask containing a magnetic stirrer, 0.02–0.04 mmol PVP was added. Then the mixture was stirred and gradually heated to 160 °C. Then 0.10–0.18 mmol $PtCl_4$ and 0.16–0.72 mmol $AgNO_3$ were successively injected into the hot solution and the heating continued for 2 h. The colour rapidly changed to black. The procedure was repeated at 160 °C, 4 h, and then for ethylene glycol at 160 °C, 3 h, 175 °C, 2 h; diethylene glycol at 190 °C, 2 h and 200 °C, 2 h. Similarly, 0.14–0.15 mmol $PtCl_4$ was used to produce Ag/Pt PET stabilized nanocomposites in aqueous solution at 90 °C.

2.3. Characterization

The nanoclusters derived by polyol stabilization were found to be very stable in both liquid and solid phases. The stability was checked by following the absorbance spectra over extended periods of several months. The oxo groups present in the vinylpyrrolidone coordinate fairly strongly to the bimetallic nanoparticles [19, 20]. The use of sodium borohydride resulted in fast reduction of metal ions, but ethane-1,2-diol was the best reducing agent and stabilizer that also acted as a solvent. A variety of techniques such as UV-Vis spectroscopy, photoluminescence (PL) spectroscopy, TEM, x-ray crystallography, and x-ray photoelectron spectroscopy (XPS) were used for the characterization of as-prepared Ag/Pt bimetallic nanoparticles.

2.3.1. Optical characterization. A Varian Cary 50 Conc UV-Vis spectrophotometer was used to carry out the optical measurements and the samples were placed in silica cuvettes (1 cm path length), using ethanol/deionized distilled water as reference solvents accordingly. A Perkin-Elmer LS 55 Luminescence spectrometer was used to measure the PL of the particles. The samples were placed in a quartz cuvette (1 cm path length).

2.3.2. Structural characterization. The crystalline phase was identified by x-ray diffraction (XRD), employing a scanning rate of 0.05° min^{-1} in a 2θ range from 20° to 80°, using a Bruker AXS D8 diffractometer equipped with nickel filtered Cu-Kα radiation ($\lambda = 1.5406$ Å) at 40 kV, 40 mA and at room temperature. The morphology and particle sizes of the samples were characterized by a JEOL 1010 TEM with an accelerating voltage of 100 kV, Megaview III camera, and Soft Imaging Systems iTEM software. The detailed morphological and structural features were investigated using HRTEM images with a JEOL 2010 transmission electron microscope operated at an accelerating voltage of 200 kV. The survey of surface property and high resolution spectra of nanoparticles were collected using x-ray photoelectron spectrometer (XPS) PHI 5000 Versaprobe–Scanning ESCA Microprobe, with 100 μm 25 W 15 kV Al monochromatic x-ray beams.

2.4. Catalysed reduction of p-nitrophenol by Ag/Pt nanoparticles in the presence of $NaBH_4$ solution

The ability of Ag/Pt nanoparticles capped or stabilized with different matrices (GLY, EG, DEG and PET) to catalyze the reduction of p-nitrophenol was investigated according to Marais and Nyokong [21], by measuring $NaBH_4$ in the presence of Ag/Pt NPs. In order to study catalytic activity, 30 mL, 10 mM of p-nitrophenol was mixed with freshly prepared 10 mL, 0.7 M aqueous solution of $NaBH_4$ with constant stirring in a 250 mL conical flask, while the temperature was maintained at 299 K. Then, 30.6 mg of as-prepared Ag/Pt PVP_{GLY} (165 °C, 4 h) nanoparticles was added to the mixture separately and the conical flask was vigorously shaken for mixing. The colour of the solution gradually changed from yellow to colourless as the reaction proceeded. The progress of the reaction was monitored by recording the UV–Vis spectra of the solutions at a time interval of 300 s. The rate constant of the reduction process was determined by measuring the change in absorbance at 400 nm as a function of time. A controlled experiment was also carried out without Ag/Pt nanoparticles and no change was noticed in the absorption spectra of 4-nitrophenol. The experiment was repeated using other Ag/Pt particles in ethylene glycol, diethylene glycol and pentaerythritol matrices.

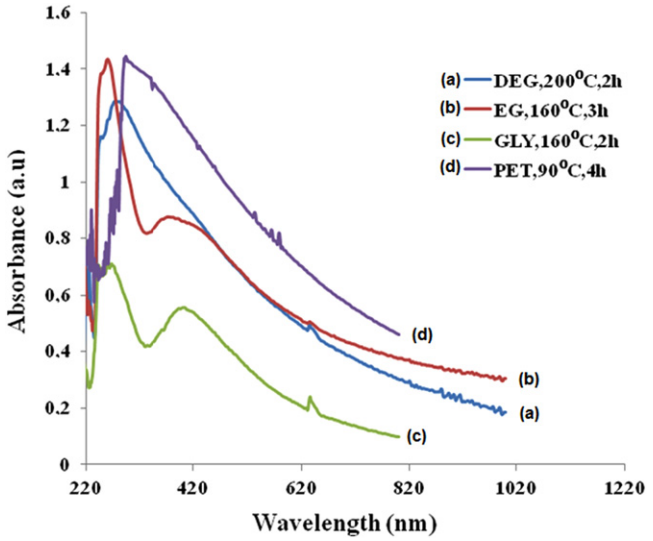

Figure 1. UV-Vis Spectra of Ag/Pt sols stabilized with PVP/DEG at 200 °C, 2 h (a); PVP/EG at 160 °C, 3 h (b); PVP/GLY at 160 °C, 2 h (c); PVP/PET at 90 °C, 4 h (d).

3. Results and discussion

3.1. Optical properties of Ag/Pt sols

The absorption spectra of allied of Ag/Pt sols stabilized with PVP/polyol matrix at controlled reaction temperatures are shown in figure 1. Similarly, the UV-Vis absorption spectra of Ag/Pt sols prepared with different mole ratios of metal Ag and Pt precursors are presented in figure 2. The absorbance spectra showed the effect of different compositions of Ag and Pt and temperature on the optical property of the Ag/Pt sols. The optimum mole ratios for the co-precipitation reactions which produced Ag/Pt sols from these metal precursors/stabilizer mixtures were 20:5:1, 26:5:1, 14:24:1 and

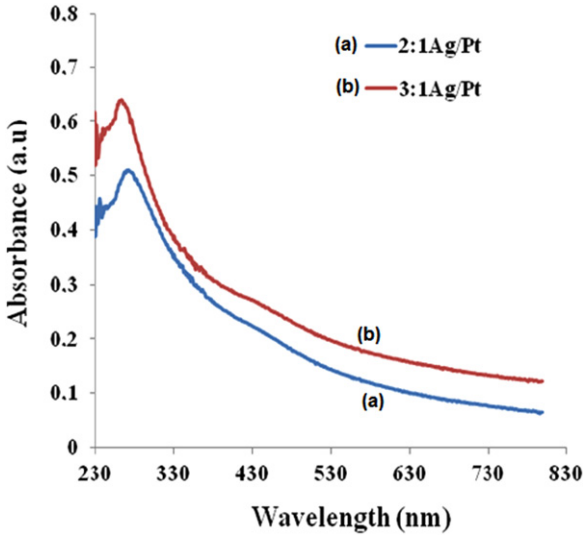

Figure 2. Absorption spectra of Ag/Pt NPs stabilized with PVP/GLY at 160 °C, 2 h for 2:1 (a) and 3:1 (b) of Ag and Pt precursors.

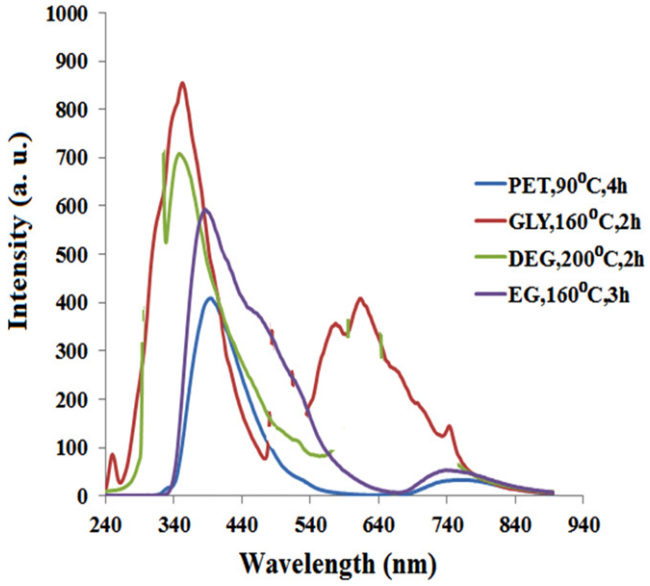

Figure 3. PL emission spectra of Ag/Pt sols showing the effect of different stabilizers.

0.60:0.15:0.04:24.78 for $Ag/Pt/PVP_{EG}$, $Ag/Pt/PVP_{GLY}$, $Ag/Pt/PVP_{DEG}$ and $Ag/Pt/PVP/PET_{BHaq}$, respectively. At these mole ratios, colloidal dispersions were formed which were easily redispersed in ethanol and the optical absorption of Ag/Pt sol was measured.

Furthermore, an alloy formation was evident by Ag/Pt sols stabilized with DEG, EG, GLY and PET due to the appearance of a single peak with their maxima strongly depending on composition. The plasmon band was blue-shifted with increasing amount of silver [22] from 280 nm to 271 nm, as seen in figure 2. The effect of different polyols also produced varying degree of blue shift in the wavelength at maximum absorbance with peaks at 264, 275, 373, and 393 nm for PVP/PET (90 °C, 4 h), PVP/DEG (200 °C, 2 h), PVP/EG (160 °C, 3 h) and PVP/GLY (160 °C, 2 h) stabilized Ag/Pt sols (figure 1), respectively. In each of these sols, the mole ratio of Ag:Pt:stabilizer were 15:4:1, 15:3:1, 20:5:1 and 25:5:1 for PET, DEG, EG and GLY matrix components, respectively. Appreciable quantum size confinement effect would be anticipated for these nanoparticles in the order of their absorption band edge shift.

The absorption band gaps of the Ag/Pt sols were also estimated by the direct band gap method [23] using the cut-off band edges (figure 1), and were found to be 2.98 eV (416 nm, $t = 2$ h), 2.88 eV (431 nm, $t = 2$ h), 2.84 eV (436 nm, $t = 3$ h) and 3.20 eV (388 nm, $t = 4$ h) for PVP/GLY, PVP/DEG, PVP/EG and PVP/PET functionalized Ag/Pt nanoparticles, respectively. The absorption edges were red-shifted from that of Ag and Pt bulk crystals given as 3.99 eV [24, 25] and 3.0 eV [26, 27], respectively.

The analysis of the optical property of as-prepared Ag/Pt sols with PL spectrometer in very dilute solution of absolute ethanol produced the emission spectra (figure 3) which showed nearly uniform peaks at 342 and 346 nm due to excitations of Ag/Pt DEG (200 °C, 2 h) and Ag/Pt GLY (160 °C, 2 h) nanoparticles, respectively, at 310 nm and 245 nm dual wavelengths. The fluorescence band, in this

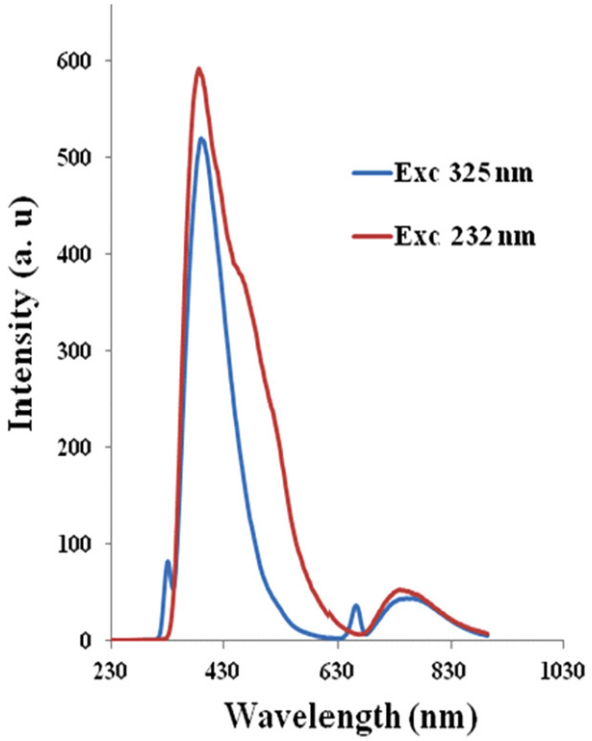

Figure 4. PL emission spectra of Ag/Pt sols stabilized with PVP/EG at 160 °C, 3 h for excitation at dual wavelengths.

instance, was significant in terms of particle size distribution, shape and energy band gap. As for PVP/EG (160 °C, 3 h) and PVP/PET (90 °C, 4 h) stabilized Ag/Pt sol, they exhibited their emission at 378 nm and 383 nm for excitation at 232 and 325 nm, respectively, which was characteristic of Ag allied sol and invariably confirmed surface enrichment of Pt by Ag nanoparticles.

The emission spectra (figure 4) also confirmed the fluorescence character of Ag/Pt sols stabilized with PVP/EG

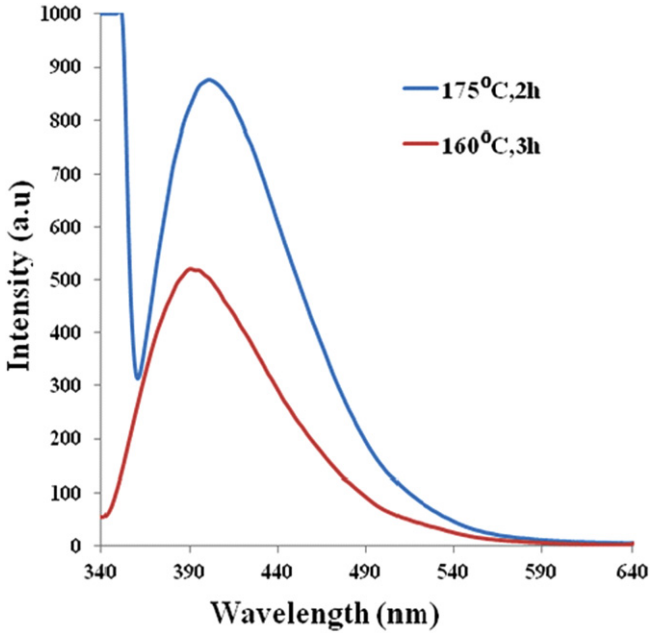

Figure 5. PL emission spectra of Ag/Pt sol stabilized with PVP/EG at 160 °C, 3 h showing the effect of change in temperature and time of reaction.

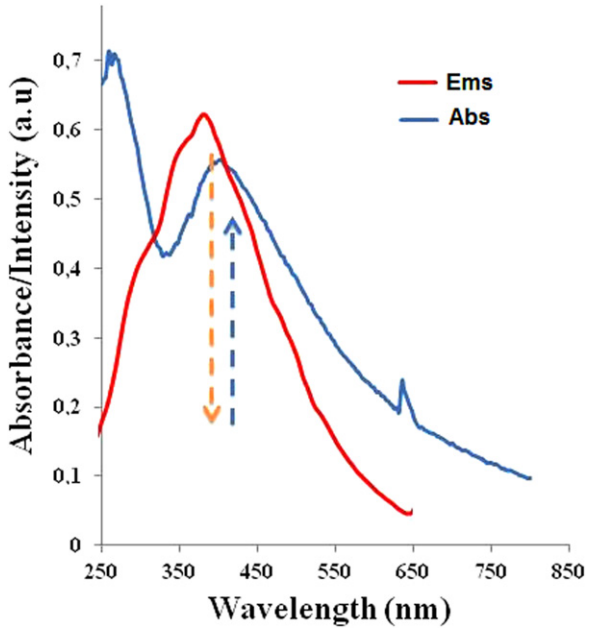

Figure 6. Combined UV-Vis and PL emission spectra of Ag/Pt GLY at 160 °C, 2 h, absorption maximum at 388 nm, PL emission at 348 nm for an excitation at 245 nm.

at 160 °C, 3 h due to dual excitation at 232 and 325 nm. There was a consistent emission at 382 nm. However, the spectra of Ag/Pt sol passivated with PVP/EG at 160 °C (figure 5) showed that an increase in temperature of reaction from 160 °C to 175 °C affected anisotropic growth of nanoparticles which resulted in very narrow and higher intensity emission peak with resultant slight red shift in the wavelength from 381 to 384 nm. Further consideration of the combined UV-Vis and PL emission spectra of Ag/Pt sols (figures 6 and 7) showed the independence of fluorescence and absorbance phenomena in Ag/Pt sols. In addition, the absorption spectrum was a mirror image of the emission spectrum which is a phenomenon of Franck Condon principle [28] ascribed to Stoke's shift.

Therefore, the refractive indices of different solvents or dispersion media have been shown to induce a shift of the surface plasmon band (SPB) as predicted by Mie theory: the maximum wavelength for a given metal cluster depends on the refractive index of the medium and it shifts to higher wavelength as refractive index of the solvent increases [29–31]. As a result, we expect appreciable quantum size confinement in these nanoparticles in the order of their optical blue shifted absorption maxima.

3.2. Morphological properties of Ag/Pt allied nanoparticles

The electron micrograph of Ag/Pt nanoparticles stabilized with different polyols produced some remarkable morphology and structures which are presented in figures 8–11. The shape and physical appearance of the new PVP/DEG, 200 °C, 2 h and PVP/EG, 160 °C, 3 h passivated Ag/Pt NPs (figures 8(a) and (b)) can best be described as hybrid nanowebs sandwiched by some quasi three- dimensional nanocubes. These

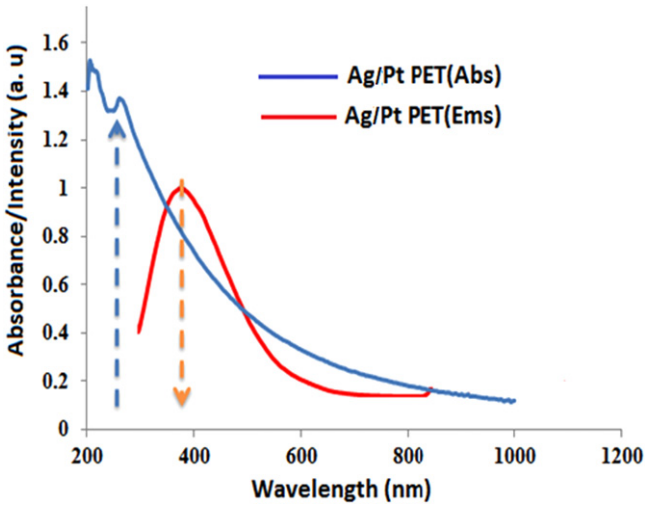

Figure 7. Combined UV-Vis/PL emission spectra of Ag/Pt PET at 90 °C, 4 h: maximum absorbance at 236 nm; PL emission at 388 nm for an excitation at 335 nm.

particles are polydispersed and the morphology of the nanocomposite varies between an alloy and core–shell formation. The nanowebs extensively evolved in PVP/EG stabilized Ag/Pt nanoparticles at 160 °C, 3 h (figure 8(b)). This unique formation can be attributed to diffusion limited growth mechanism [32] which was facilitated by hot precipitation with ethanol and also etching, made possible by the interaction of chloride ion and oxygen from air with Ag^{+} and Pt^{4+} ions during anisotropic reduction, nucleation and growth processes [33, 34]. The mean diameter of the sandwiched nanocubes was 30.45 nm ± 6.23 nm.

Similarly, the shape and morphology of the PVP/GLY, 160 °C, 4 h stabilized Ag/Pt NPs (figure 9(a)) consisted of an

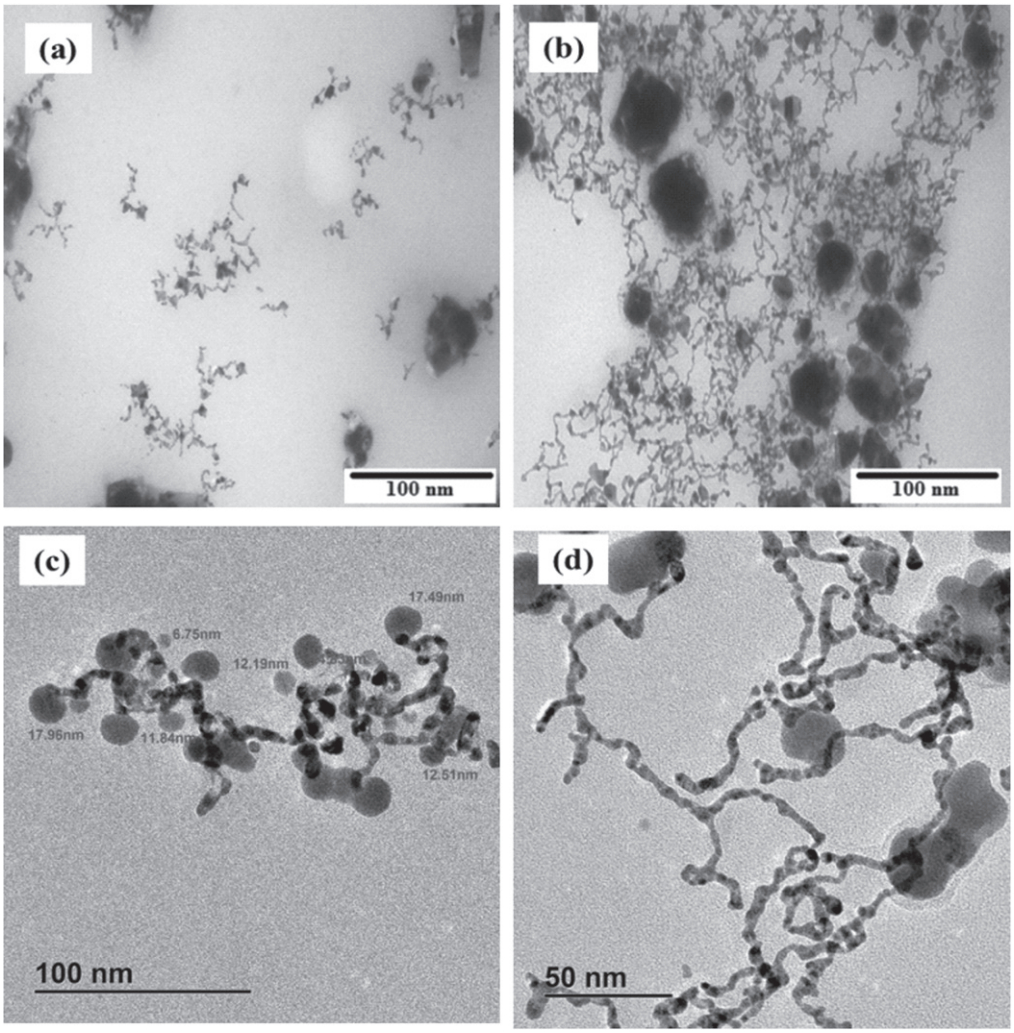

Figure 8. TEM images of Ag/Pt NPs stabilized with (a) PVP/DEG at 200 °C, 2 h; (b) PVP/EG at 160 °C, 3 h; (c), (d) HRTEM images of (a), (b), respectively.

alloy structure in which there was an edge to edge attachment of the nanocomposites. The nanowebs appeared to be rudimentary and not well developed, while the 160 °C, 2 h stabilized nanocomposite (figure 9(b)) showed the evolution of wormlike nanowires with a mean particle size of 26.43 nm ± 4.87 nm. The difference in morphology showed that reaction time played a significant role in anisotropic growth of Ag/Pt nanoparticles [35]. Moreover, HRTEM analysis of Ag/Pt NPs functionalized with PVP/PET at 90 °C, 4 h (figure 10) showed that highly crystalline uniformly dispersed nanocubes with delineated edges were formed. The mean particle size was 18.54 nm ± 1.76 nm, and the morphology based on HRTEM image (figure 10(b)) confirmed the formation of an alloy with a periodic array typical of Ag and Pt nanocomposites.

Furthermore, the HRTEM images of PVP/GLY stabilized Ag/Pt at 160 °C, 2 h (figures 9(c) and (d)) confirmed the crystalline nature of the nanocomposites. The interplanar distance or lattice spacing was 2.34 Å. The image (figure 9(d)) showed two overlapping planes due to {111} Pt and {111}Ag. By making reference to transmission electron microscope (TEM) results, the growth of nanowires and nanowebs underwent an oriented attachment process which was largely thermodynamically driven, resulting in equilibrium between the binding energy of the stabilizing matrix (PVP) on the alloy surface and the diffusion of atoms at the interface upon collision of primary nanoparticles [36]. However, for Pt and Ag, the influence from various factors is conflicting. On one hand, the potential energy gain upon collision of Ag nanoparticles is smaller than that of Pt nanoparticles, indicating that the collision between Ag nanoparticles is less likely to occur.

In figure 10, images (c), (d) of Ag/Pt nanoparticles stabilized with ethylene glycol at 160 °C, 3 h revealed the pseudo crystalline nature of the nanocluster. A core–shell structure was equally evident in which Pt nanowire was enriched on the surface by Ag nanocubes of very finite dimension from 6.75 nm to 17.49 nm. For further consideration of Ag/Pt nanocluster passivated with PVP/DEG at 200 °C, 2 h, figure 11 shows the formation of long chainlike rigid backbone structure formed as a result of seed growth mechanism which produced these lattice oriented interplanar attachments of Pt with the deposition of Ag on the surface.

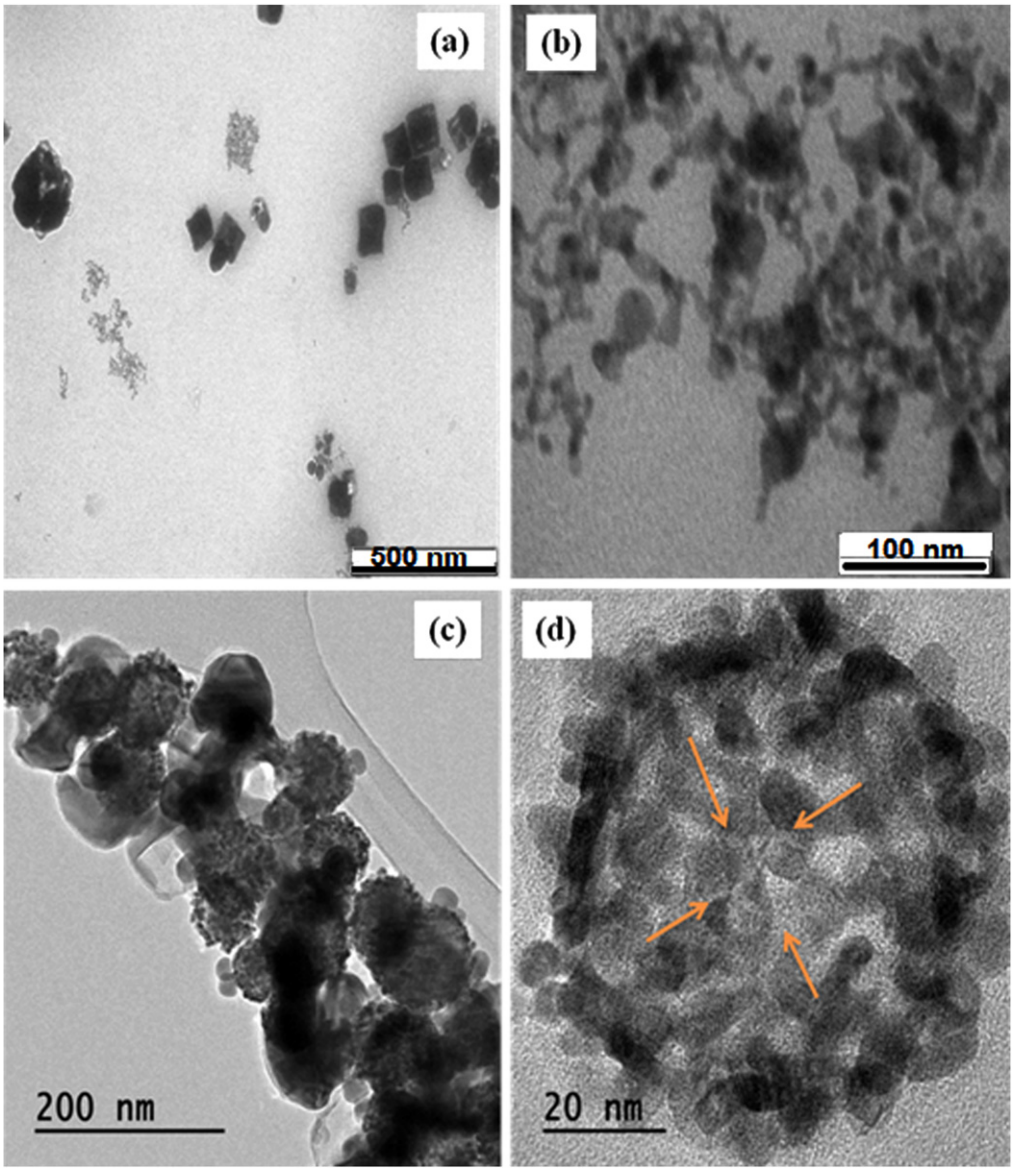

Figure 9. TEM images of Ag/Pt NPs stabilized with (a) PVP/GLY at 160 °C, 4 h and (b) PVP/GLY at 160 °C, 2 h; (c), (d) HRTEM images of Ag/Pt NPs stabilized with PVP/GLY at 160 °C, 2 h.

The powder x-ray diffraction (p-XRD) patterns of as-prepared Ag/Pt nanoparticles in different polyols are shown in figure 12. The Ag/Pt nanoparticles stabilized with PVP/GLY at 160 °C, 2 h (figure 12(a)) had the strongest reflection at $2\theta = 40.07°$. This value was significantly higher than that of either face-centered cubic (fcc) Pt or (fcc) Ag. The fcc {111} Pt diffraction planes occurred at $2\theta = 39.91°$ [37], while fcc Ag {111} characteristic peak appeared at $2\theta = 38.42°$ [38]. The unit cell length of the Ag/Pt nanoparticles stabilized by PVP/DEG at 200 °C, 2 h (figure 12(b)) based on the calculation at {111} diffraction planes being 28.83 nm which was larger than that of Ag, 25.56 nm or Pt, 8.06 nm. This indicated that Ag/Pt nanoparticles had a non-conventional fcc lattice. This shift does not fit into Vegard's law [39]. The Ag/Pt nanocomposite should have a unit length in between the two elements. The shoulder peak at $2\theta = 46.52°$ which was assigned to {002} Pt diffraction plane of fcc lattice structure was very pronounced, while, the peaks at 2θ being 44.45° and 76.37° attributed to {200} and {311} planes of Ag were also relatively higher than 2θ reflections of bulk Ag. Meanwhile, the peak at $2\theta = 38.42°$ assigned to {111}Ag was almost extinct. Similar peaks and diffraction patterns were exhibited by Ag/Pt NPs stabilized with PVP/EG at 160 °C, 3 h (figure 12(c)). Similarly, diffractions of the {111} and {222} planes assigned to Ag were absent from reflection peaks of PVP/PET capped Ag/Pt NPs (figure 12(d)), whereas other peaks appeared at 2θ being 46.50° and 67.67°, supporting the proposition of core–shell structure for the allied nanoparticles.

The p-XRD patterns of the Ag/Pt nanocomposites prepared at the mole ratios of 15:3:1, 20:5:1, 25:5:1 and 15:4:1 for DEG, EG, GLY and PET stabilized matrices, respectively, exhibited nanoalloy structures. The differentiated peaks

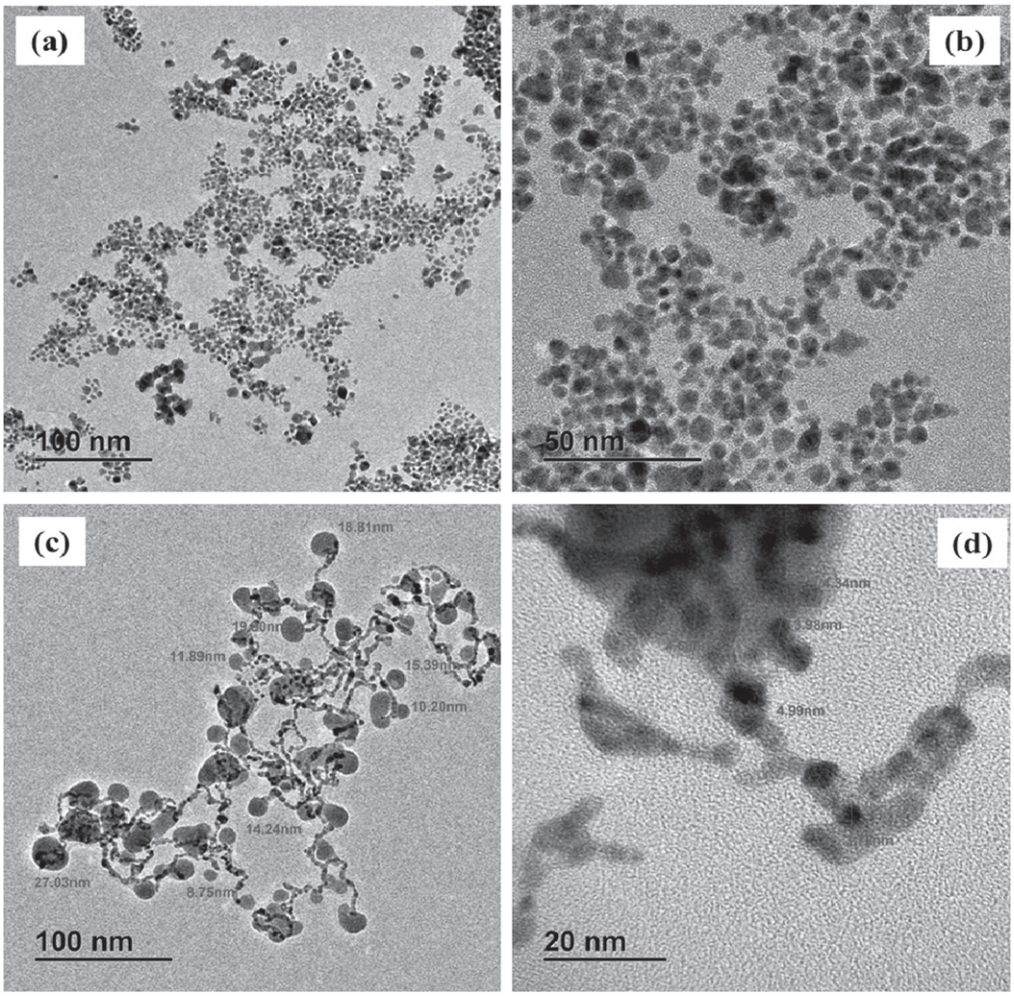

Figure 10. (a), (b) HRTEM images of Ag/Pt NPs stabilized with (a) PVP/PET at 90 °C, 4 h; (c), (d) HRTEM images of Ag/Pt NPs stabilized with PVP/EG at 160 °C, 3 h showing nano alloy hybrid morphology.

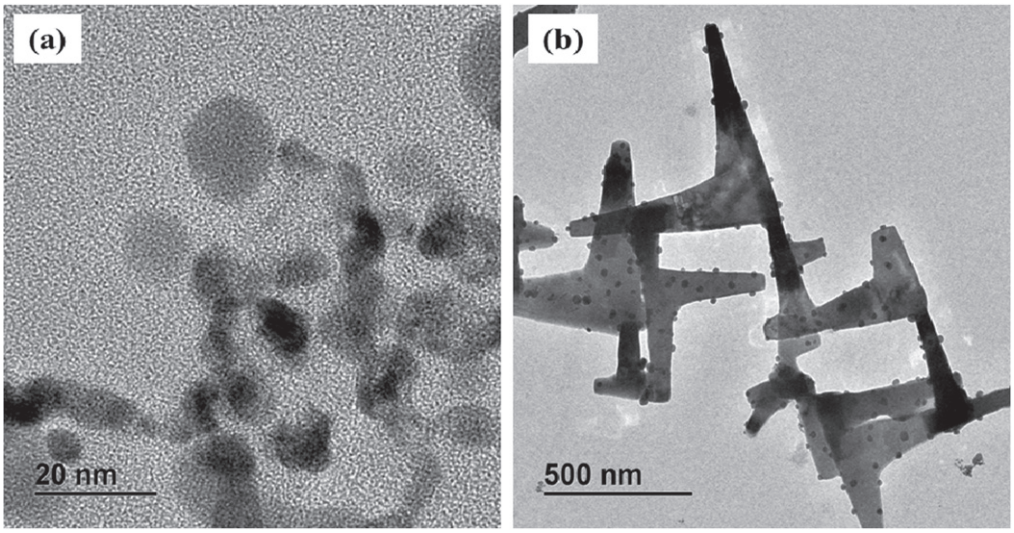

Figure 11. HRTEM images of Ag/Pt NPs stabilized with PVP/DEG at 200 °C, 2 h showing nano alloy hybrid morphology.

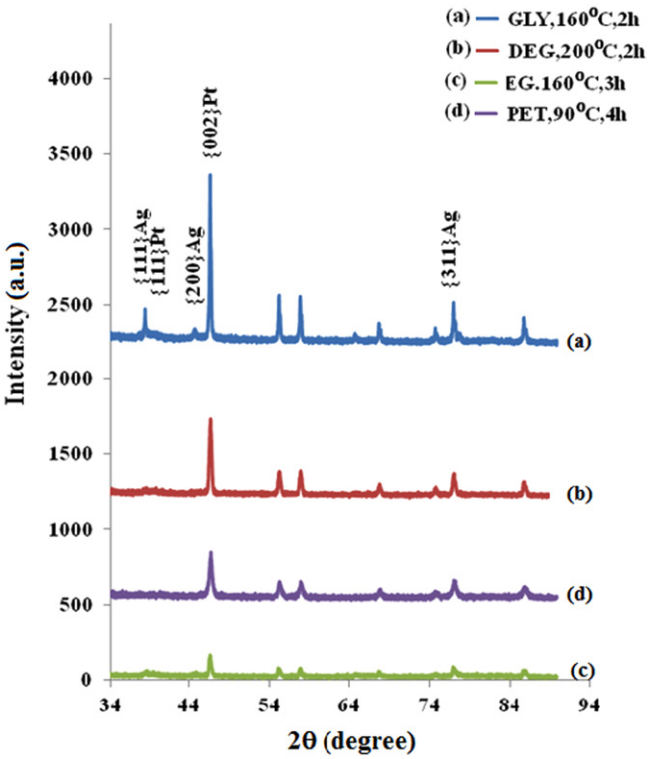

Figure 12. P-XRD patterns showing the polycrystalline nature of Ag/Pt nanoparticles stabilized with (a) PVP/GLY at 160 °C, 2 h; (b) PVP/DEG at 200 °C, 2 h; (c) PVP/EG at 160 °C, 3 h; (d) PVP/PET at 90 °C, 4 h.

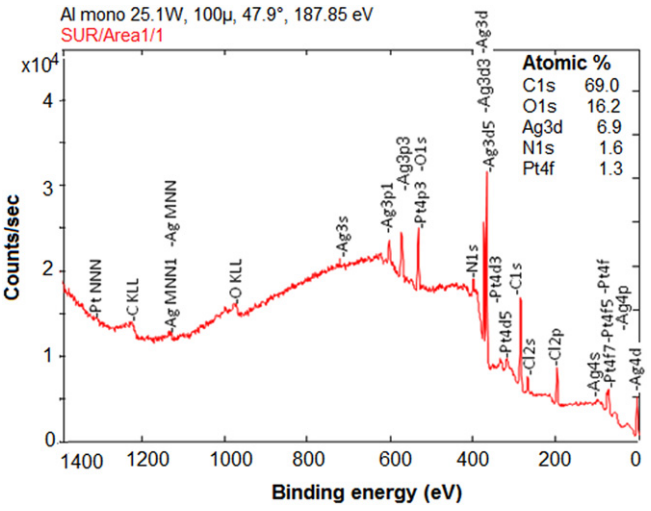

Figure 13. XPS spectrum of high resolution scan of Ag/Pt nanoparticles stabilized with PVP/DEG at 200 °C, 2 h.

strongly supported the crystallinity and polydispersity of Ag/Pt nanoparticles formed with some measures of lattice contraction [40].

3.3. XPS result of Ag/Pt in polyols.

For the XPS analysis, one of the Ag/Pt nanoparticles was considered for characterization with sputtering at the surface monolayers. The spectrum and the high resolution scans of

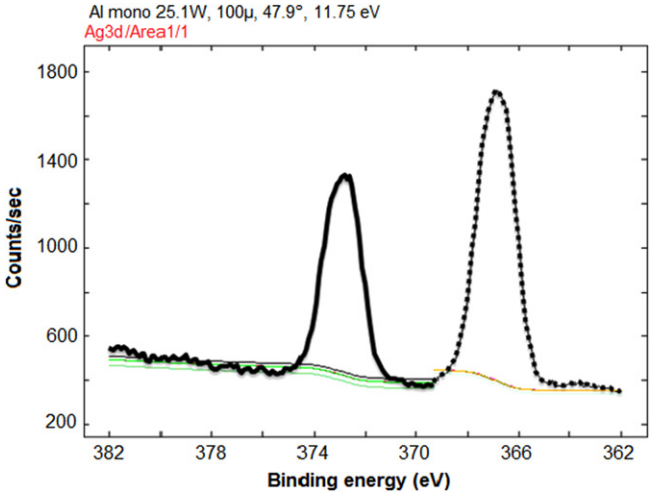

Figure 14. High resolution scan of Ag(3d) core levels of Ag/Pt nanoparticles stabilized with PVP/DEG at 200 °C, 2 h.

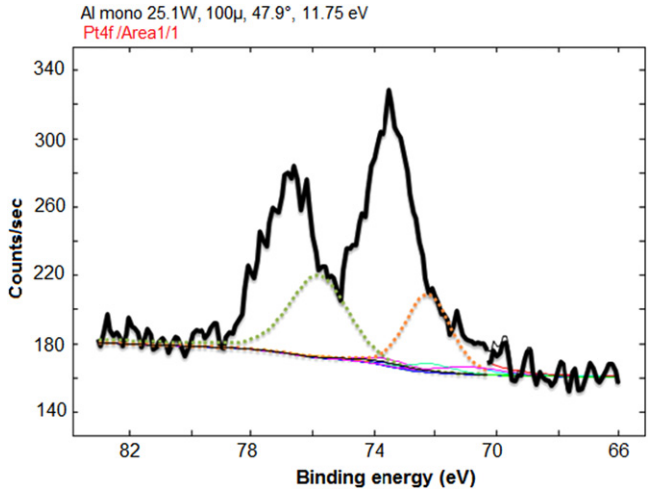

Figure 15. High resolution scan of Pt(4f) core levels.

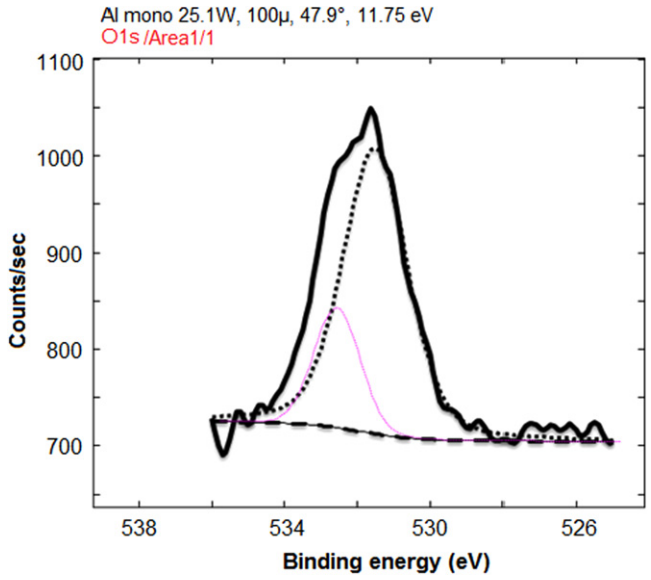

Figure 16. High resolution scan of O(1s) core levels.

the core levels of Ag/Pt nanoparticles are presented in figures 13–16. The elemental composition and the oxidation state of the prepared nanocomposites were analysed with an analytical XPS instrument. The survey scan of Ag/Pt NPs stabilized with PVP/DEG at 200 °C, 2 h, figure 13 indicated the presence of Ag, Pt, and O according to their binding energies. It was observed that the atomic ratio of Ag to Pt in the prepared nanocomposites from XPS data was 6.91:1.32 which strongly agreed with the mole ratio of metal precursors used. It further confirmed the successful formation of nanoalloy structure. In addition, the integration of the peaks also showed a very high intensity for Ag metal.

Furthermore, the Ag ($3d_{5/2}$) component, figure 14 had a lower binding energy (BE) compared to pure Ag metal. It was resolved at 368.02 eV (BE), while the binding energy of pure Ag metal was 368.2 eV [41]. The shift was as a result of the bond formed with Pt or O. The evidence of Ag bonding with either Pt or O arose from the deconvolution of XPS high resolution scan for individual bonding atoms. The Ag(3d) core was found to split as a doublet with a second peak at 366.84 eV (BE) which was assigned to lattice oxygen (O) of AgO. Similarly, the Pt ($4f_{7/2}$) core level, figure 15 splits into a quartet while ($4f_{5/2}$) component splits as doublet. The characteristic splitting of Pt produced four unique peaks with binding energies of 71.14, 72.15, 73.65 and 74.84 eV. The first two were assigned to Pt^0 metal atom, while subsequent ones were resolved as parametric peaks [42] for PtO and PtO_2, respectively.

Likewise, the deconvoluted XPS high resolutions scan for O (1s) levels (figure 16) split as a triplet. The main peak centered at 531.22 eV (BE) was attributed to PtO [42, 43] in the $AgPtO_x$ structure. The peak at 531.22 eV was associated with the O (1s) in the AgO species. According to a previous study [44], the peak of O(1s) at 530.9 eV was indexed to the lattice oxygen (OL) of PtO since this oxygen had a partial negative charge that shifted the photoelectron line to lower binding energy. Therefore, $AgPtO_x$ possessed a cluster-in-cluster alloy structure with more of the core occupied by Ag^0 metal, while Pt^0 dominated the domains.

3.4. Result of catalysis study

The catalytic conversion of the 4-nitrophenol to 4-aminophenol on addition of Ag allied nanobimetallic particles (Ag/Pt/PVP/polyol) was quantitatively monitored as a successive decrease in the peak height at 400 nm (figure 17) and the gradual development of new peak at 300 nm which validated the formation of 4-aminophenol [45], corresponding to a change in solution colour from light yellow to yellow-green. In this experiment, the concentration of the borohydride ion used as reductant, largely exceeded that of 4-nitrophenol.

The mechanism of the reduction is such that, the Ag/Pt/PVP/polyol stabilized nanoparticles started the catalytic reduction by relaying electrons from the donor BH_4^- to the acceptor 4-nitrophenol after the adsorption of both onto the particles surfaces. Since the ratio of absorbance (A) of 4-nitrophenol at time t to its value A_0 measured at $t = 0$ (close to infinity) must be equal to the concentration ratio C_t/C_0 of 4-nitrophenol, the kinetic equation for the reduction can be written as

$$\frac{\partial C_t}{\partial t} = -k_{app} C_t,$$

$$\ln \frac{C}{C_0} = \ln \frac{A}{A_0},$$

where C_t is the concentration of 4-nitrophenol at time t, and k_{app} is the apparent rate constant, which can be obtained from the decrease of the peak intensity at 400 nm with time. A good linear fitting of ln (A/A_0) versus the reaction time was obtained, indicating that pseudo-first-order kinetic could be used to calculate the kinetic rate constant. Figure 18 shows a

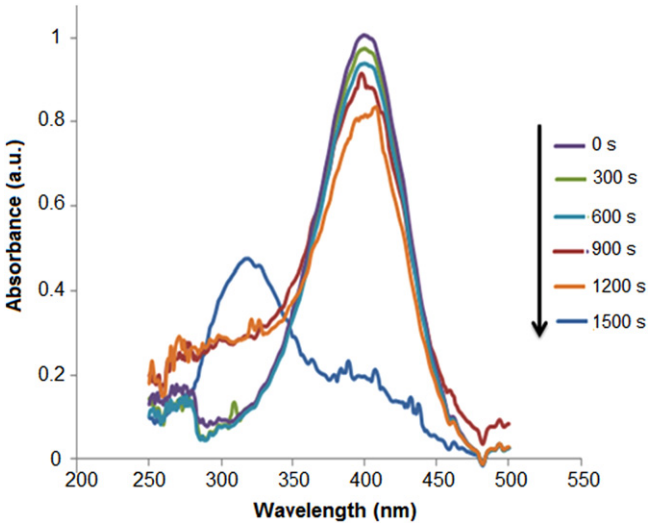

Figure 17. Change in absorbance at 400 nm as a function of time using Ag allied nanobimetallic particles prepared as catalysts Ag/Pt in PVP/GLY at 160 °C, 4 h.

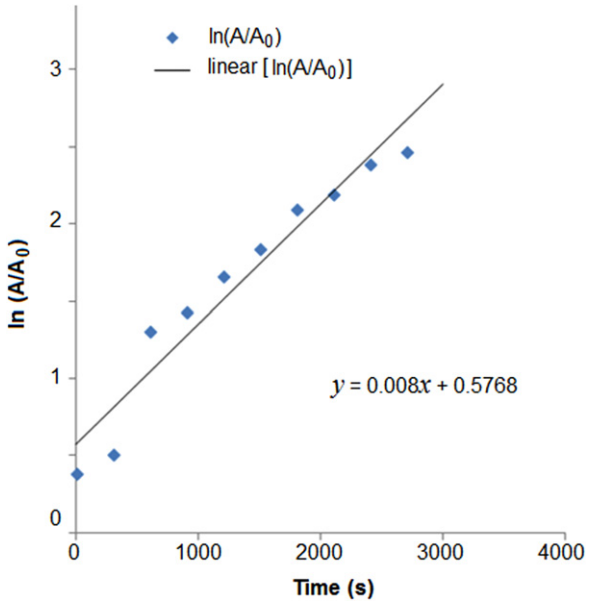

Figure 18. Plots of ln(A/A_0) and the reaction time t(s) at 299 K for Ag/Pt in PVP/GLY 165 °C, 4 h.

Table 1. Summary of observed rate constant of Ag/Pt allied nanoparticles.

Ag/Pt nanobimetallic particles	Observed rate constant (s^{-1})
Ag/Pt/PVP/GLY, 160 °C, 2 h	3.1×10^{-3}
Ag/Pt/PVP/GLY, 160 °C, 4 h	8.0×10^{-4}
Ag/Pt/PVP/DEG, 200 °C, 2 h	4.8×10^{-3}
Ag/Pt/PVP/EG, 160 °C, 3 h	6.0×10^{-4}
Ag/Pt/PVP/PET/BH_4^-, 90 °C, 4 h	1.2×10^{-3}

linear correlation between $\ln(A/A_0)$ and the reaction time t at 299 K, indicating that the reaction is a pseudo-first-order.

There is an increase in kinetic rate constant when bimetallic nanoparticles are used as catalysts instead of their monometallic analogues. Looking at the observed rate constants of 4-nitrophenol catalysed reduction at 299 K, Ag/Pt/PVP/DEG catalyst exhibited a rate constant of 4.8×10^{-3} s^{-1} (table 1) which is significantly higher than 2.8×10^{-3} s^{-1} reported for Poly(ethylenimine)-Stabilized Ag nanoparticles [46, 47]. However, Ag/Pt/PVP/PET (reduced by $NaBH_4$ in aqueous phase at 90 °C, 4 h), Ag/Pt/PVP/GLY (160 °C, 4 h) and Ag/Pt/PVP/EG (160 °C, 3 h) catalysts were among those with minimum values of rate constant of 1.2×10^{-3} s^{-1}, 8.0×10^{-4} s^{-1} and 6.0×10^{-4} s^{-1}, respectively.

In accounting for this observed difference, let us consider the atomic ratio, characteristic size, shape and structure of nanobimetallic particles precipitated by co-reduction in aqueous and non-aqueous solutions. In principle, polymer stabilized nanocatalysts precipitated from aqueous phase are more crystalline than those precipitated from non-aqueous solution. Nanostructured amorphous bimetal catalysts strongly adsorb BH_4^- ion and 4-NP onto their surfaces and in so doing rapidly facilitate reduction to 4-AP.

As a result, adsorption at interfacial surface, especially within the 100 crystallographic planes largely depends on surface porosity, the total surface area of strongly adsorbing species (reduced and nanosized Ag^0 or Pt^0 metal) and the nature of chemical interaction involved as a result of hydrophobicity of the nanoparticles [48–50]. In fact, Ag/Pt PVP/DEG with the highest rate constant, has a mole ratio of 0.52:0.12 and particle size of 4.59 nm and surface atomic composition of Ag/Pt from XPS data, 5:1 which strongly suggests a cluster in cluster in which each Pt and Ag atoms are randomly alloyed together.

4. Conclusion

The synthesis of silver platinum nanobimetallic particles by co-reduction and co-precipitation from non-aqueous and aqueous solutions using molecular source precursors and polymer encapsulation matrices has been accomplished. Subsequently, characterization of as-prepared nanocomposites was done using optical spectroscopy, electron microscopy, x-ray diffraction (XRD) and x-photoelectron spectroscopy methods. However, a novel material was formed when Ag/Pt was segregated from solution by hot addition of absolute ethanol; the result when viewed by TEM image revealed quasi nanocubes entangled in nanowebs which has not been previously reported. The nanocube measured 30.45 ± 6.23 nm which is evidently 3D quantized. Looking at the catalytic reduction of 4-nitrophenol at 299 K, Ag/Pt/PVP_{COH} nanocatalysts investigated, they exhibited relatively higher rate constant than monometallic Ag nanoparticles, showing the significant input of new nanocomposite material.

Acknowledgements

The authors are grateful to the National Research Foundation (NRF), Department of Science and Technology (DST) South Africa. The authors also thank Dr James Wesley-Smith from the Electron Microscopy Unit, University of Kwa-Zulu Natal for TEM measurements and CSIR, Pretoria for HRTEM facility and Professor Hendrik Swart of the Department of Physics, University of Free State, Bloemfontein, South Africa for XPS analysis.

References

[1] Gao J, Ren X, Chen D, Tang F and Ren J 2007 *Scripta Mater.* **57** 687
[2] He Y Q, Zeng K, Gurung A S, Baloda M, Xu H and Zhang X 2010 *Anal. Chem.* **82** 69
[3] Devarajan S, Bera P and Sampatha S 2005 *J. Colloid Interface Sci.* **290** 117
[4] Sun X, Dong S and Wang E 2004 *Macromolecules* **37** 7105
[5] Xia Y, Xiong Y, Lim B and Skrabalak S E 2008 *Angew. Chem. Int. Ed.* **48** 60
[6] Wu M and Lai L 2004 *Colloid. Surface. A: Physicochem. Eng. Aspects* **244** 149
[7] Wen-Yin K, Jun-Wei S, Chian-Hua G and Kuan-Jiuh L 2012 *Carbon* **50** 2244
[8] Gao J, Ren X, Chen D, Tang F and Ren J 2007 *Scr. Mater.* **57** 687
[9] Chena L, Zhaoa W, Jiaoa Y, Hea X, Wanga J and Zhanga Y 2006 *Spectrochim. Acta* A **68** 484
[10] You H, Peng Z, Wu J and Yang H 2011 *Chem. Commun.* **47** 12595
[11] Cushing B L, Kolesnichenko V L and O'Connor C J 2004 *Chem. Rev.* **104** 3893
[12] Viau G, Brayner R, Poul L, Chakroune N, Lacaze E, Fievet-Vincent F and Fievet F 2003 *Chem. Mater.* **15** 486
[13] Toshima N, Kushihashi K, Yonezawa T and Hirai H 1989 *Chem. Lett.* **18** 1769
[14] Toshima N, Yonezawa T and Kushihashi K 1993 *J. Chem. Soc. Faraday Trans.* **89** 2537
[15] Yang J, Lu L, Wang H and Zhang H 2006 *Scripta Mater.* **54** 159
[16] Vasquez Y, Sra A K and Schaak R E 2005 *J. Am. Chem. Soc.* **127** 12504
[17] Yonezawa T and Toshima N 1993 *J. Mol. Catalysis* **83** 167
[18] Toshima N, Kanemaru M, Shiraishi Y and Koga Y 2005 *J. Phys. Chem.* B **109** 16326
[19] Lu P, Teranishi T, Asakura K, Miyake M and Toshima N 1999 *J. Phys. Chem.* B **103** 9673
[20] Jiang H, Moon K, Li Y and Wong C P 2006 Ultra high conductivity of isotropic conductive adhesives *Proc. of the 56th Institute of Electrical and Electronics Engineers (IEEE) Electronic Components and Technology Conf. (San Diego, CA, May 30-June 2, 2006)* pp 485–90

[21] Marais E and Nyokong T 2008 *J. Hazard. Mater.* **152** 293
[22] Kassab L R P, de Araújo C B, Kobayashi R A, de Almeida Pinto R and da Silva D M 2007 *J. Appl. Phys.* **102** 103515
[23] Hoffman M, Martin S, Choi W and Bahnemann D 1995 *Chem. Rev.* **95** 69
[24] Kim S S, Na S I, Jo J, Kim D Y and Nah Y C 2008 *Appl. Phys. Lett.* **93** 073307
[25] Koichi A, Makoto F, Carsten R, Junji T, Hirotaka M, Yoshimichi O, Naoya Y and Toshiya W 2008 *Am. Chem. Soc.* **130** 1676
[26] Wilson J S, Kohler A, Friend R H, Al-Suti M K, Al- Mandhary M R A, Khan M S and Raithby P R 2000 *J. Chem. Phys.* **113** 7627
[27] Kohler A, Wilson J S, Friend R H, Al-Suti M K, Khan M S, Gerhard A and Bassler H 2002 *J. Chem. Phys.* **116** 9457
[28] Lakowicz J R 2006 *Principles of Fluorescence Spectroscopy* 3rd ed (Berlin: Springer) pp 5–8
[29] Ingle A, Gade A, Pierrat S, Sonnichsen C and Rai M 2008 *Current Nanosci.* **4** 141
[30] Templetou A C, Pletron J J, Murray R W and Mulvaney P 2000 *J. Phys. Chem.* B **101** 564
[31] Underwood S and Mulvaney P 1994 *Langmuir* **10** 3427
[32] Wang D and Li Y 2011 *Adv. Mater.* **23** 1044
[33] Dare E O *et al* 2012 Zinc salt-mediated synthesis, growth kinetic, and shaped evolution of silver nanoparticles *ISRN Nanomaterials* **2012** 376940
[34] Adekoya J A, Dare E O, Mesubi M A, Nejo A A, Swart H C and Revaprasadu N 2014 *Res. Phys.* **4** 12–9
[35] Yuan Q, Zhuang J and Wang X 2009 *Chem. Commun.* **43** 6613
[36] Xiong Y and Xia Y 2007 *Adv. Mater.* **19** 3385
[37] Wu J, Gross A and Yang H 2011 *Nano Lett.* **11** 798
[38] Pingali K C, Rockstraw D A and Deng S G 2005 *Aerosol Sci. Technol.* **39** 1010
[39] Peng Z M and Yang H 2008 *J. Solid State Chem.* **181** 1546
[40] Hofmeister H 2007 *J. Optoelectron. Adv. Mater.* **9** 99–105
[41] Kumar V and Yadav S K 2009 *J. Chem. Tech. Biotech.* **84** 151
[42] Moulder J F, Stickle W F, Sobol P E and Bomben K D 1995 *Handbook of X-ray Photoelectron Spectroscopy* ed J Chastain and R C King Jr (Chanhassen, MN: Physical Electronics Inc.)
[43] Bedyal A K, Kumar V, Sharma V, Pitale S S, Coetsee E, Dovenhage M M, Ntwaeaborwa O M and Swart H C 2013 *J. Mater. Sci.* **48** 3327
[44] Tam K H, Cheung C K, Leung Y H, Djurisic A B, Ling C C, Beling C D, Fung S, Kwok W M, Chan W K and Phillips D L 2006 *J. Phys. Chem.* B **110** 20865
[45] Rashid M H, Bhattacharjee R R, Kotal A and Mandal T K 2006 *Langmuir* **22** 7141
[46] Abdelsayed V, Aljarash A and El-Shall M S 2009 *Chem. Mater.* **21** 2825
[47] Shin M K, Lee B, Kim S H, Lee J A, Spinks G M, Gambhir S, Wallace G G, Kozlov M E, Baughman R H and Kim S J 2012 *Nature Commun.* **3** 650
[48] Park J Y, Zhang Y, Grass M, Zhang T and Somorjai G A 2008 *Nano Lett.* **8** 673
[49] Smetana A B, Klabunde K J, Sorensen C M, Ponce A A and Mwale B J 2006 *J. Phys. Chem.* B **110** 2155
[50] Sun Y and Xia Y 2004 *J. Am. Chem. Soc.* **126** 3892